Geotechnical Aspects of Underground Construction in Soft Ground – Yoo, Park, Kim & Ban (Eds)
© 2014 Korean Geotechnical Society, Seoul, Korea, ISBN 978-1-138-02700-8

Numerical modelling of ground improvement techniques considering tension softening

H.F. Schweiger & Pouya Sedighi
Graz University of Technology, Graz, Austria

S. Henke & K.-M. Borchert
GuD Geotechnik und Dynamik Consult GmbH, Berlin, Germany

ABSTRACT: Ground improvements methods such as mixed-in-place and jet grouting techniques have proven to be efficient auxiliary measures for deep excavations constructed in poor ground conditions. Although the design is primarily based on empirical rules, numerical methods are frequently employed in order to assess the deformation behaviour of these structures, but increasingly also to evaluate the stress state in the treated soil. This requires the use of appropriate constitutive models capturing the main features of the mechanical behaviour, notably their limiting tensile strength and initiation of cracks. In this paper a newly developed constitutive model is applied to simulate the behaviour of a jet grout panel supporting a deep excavation against uplift pressure. It could be shown that a reliable estimation of the stress distribution and crack patterns in the slab can be obtained providing a basis for optimization with respect to tension piles or geometry of the jet grout slab.

1 INTRODUCTION

Ground improvements methods such as stone columns, cemented stone columns, mixed-in-place and jet grouting techniques have proven to be efficient for improving the mechanical behaviour of soft ground. Although the design of ground improvement techniques is primarily based on empirical rules, numerical methods are frequently employed in order to assess the deformation behaviour of these structures, but increasingly also to evaluate the stress state in the treated soil. One of the key aspects of this type of analysis is the constitutive model employed for describing the mechanical behaviour of the improved ground. Simple elastic-perfectly plastic failure criteria are often applied in practice (see e.g. Borchert et al., 2013) but these models cannot capture important aspects of the mechanical behaviour of such materials, in particular when the tensile strength is exceeded. Therefore either significant engineering judgement is required to interprete the results or the model parameters have to be changed manually during the analysis to take into account e.g. the development of cracks. It should be emphasized that in general cemented, mixed-in-place and jet grout columns are not reinforced.

With respect to modelling the mechanical behaviour of cemented materials some researchers have developed models utilizing concepts employed for modelling structured soils (e.g. Gens & Nova, 1993). These models are usually extensions of Cam Clay type models (e.g. Horpibulsuk et al., 2010) or modifications of it, see e.g. Arroyo et al. (2012) who employ the CASM (Clay and Sand Model) developed by Yu (1998). Although this approach has proven to be successful it is not well suited to model concrete-like materials such as jet grout and mixed-in-place columns because these materials behave like weak concrete where modelling of tensile strength and tension softening becomes important. For this reason strength criteria based on the Mohr-Coulomb failure criterion with tension cut-off,occasionally enhanced to include viscous effects (e.g. Kudella et al., 2003), or empirical formulations (e.g. Fang et al., 1994) have been proposed in the past.

In this paper a newly developed constitutive model for shotcrete is applied for modelling jet grout material. It could be shown that with the appropriate choice of parameters this model is well capable of modelling important features of the mechanical behaviour of jet grout material. One of the key features of the model is the capability of accounting for tension softening. It is well known that this type of behaviour cannot be modelled in a standard finite element approach and therefore fracture energy regularization is suggested. Only a brief summary of the model is presented here because the emphasis of this paper is to prove the applicability to practical geotechnical engineering by solving a, slightly simplified, problem of a deep excavation involving a jet grout slab and tension piles. The influence of various modelling assumptions is discussed and the potential of the model for optimizing the design is shown. For the post tension region only very limited data is available and therefore the consequences of different assumptions are highlighted.

Table 1. Parameters of the "shotcrete" model.

Name	Unit	Remarks
E_{28}	[kN/m^2]	Young's modulus after 28d
ν	[–]	Poisson's ratio
$f_{c,28}$	[kN/m^2]	uniaxial compressive strength after 28d
$f_{t,28}$	[kN/m^2]	uniaxial tensile strength after 28d
ψ	[°]	angle of dilatancy
E_1/E_{28}	[–]	ratio of Young's modulus after 1d and 28d
$f_{c,1}/f_{c,28}$	[–]	ratio of f_c after 1d and 28d
f_{c0n}	[–]	normalized initial yield stress (compr.)
f_{cfn}	[–]	normalized failure strength (compr.)
f_{cun}	[–]	normalized residual strength (compr.)
ε_{cp}^{p}	[–]	plastic peak strain in uniaxial compression at shotcrete ages of 1 h, 8 h and 24 h
$G_{c,28}$	[kN/m]	fracture energy in compression after 28d
f_{tun}	[–]	normalized residual tensile strength
$G_{t,28}$	[kN/m]	fracture energy in tension after 28d
φ^{cr}	[–]	ratio of creep vs. elastic strains
t_{50}^{cr}	[–]	time at 50% of creep
$\varepsilon_{\infty}^{shr}$	[–]	final shrinkage strain
t_{50}^{shr}	[–]	time at 50% of shrinkage

Emphasis is placed on the development of crack patterns. Although this usually does not have a severe impact on the global safety of the structure it is worthwhile to take these effects into account in the numerical analysis in order to have additional information for designing the required thickness of the jet grout panel.

2 CONSTITUTIVE MODEL FOR JET GROUT MATERIAL

The constitutive model applied in this study to model the mechanical behaviour of jet grout material is essentially the same as presented in detail by Schaedlich & Schweiger (2014) for modelling the behaviour of shotcrete, whereas a few features, available in the model but not required for the purpose of this study, are switched off. As mentioned previously, emphasis is put here on the development of cracks once the tensile strength is exceeded. The model has been implemented in the finite element software PLAXIS 2D 2012 (Brinkgreve et al. 2012) and only the key features are briefly described in the following.It is noted that a compression negative notation is employed throughout the paper.

2.1 *Model parameters*

The complete list of input parameters for the model is summarised in Table 1.

2.2 *Yield surfaces and strain hardening/softening*

Plastic strains are calculated according to strain hardening/softening elastoplasticity. The model

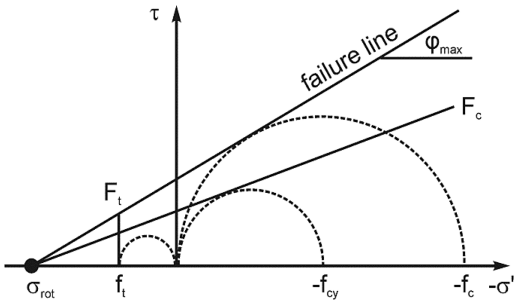

Figure 1. Yield surfaces and failure envelope.

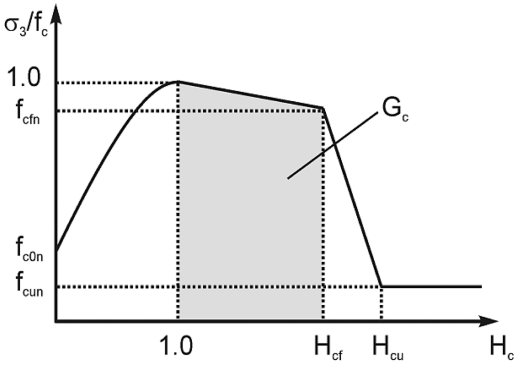

Figure 2. Normalized stress–strain curve in compression.

employs a Mohr-Coulomb yield surface F_c for deviatoric loading and a Rankine yield surface F_t in the tensile regime (Fig. 1). In this study constant values of $\varphi_{max} = 37°$ and $\psi = 0°$ are employed.

Strain hardening in compression follows a quadratic function up to the peak strength, with subsequent bi-linear softening, but compression softening is not considered in this study (Fig. 2). Due to the time dependency of the involved material parameters, a normalised hardening/softening parameter $H_c = \varepsilon_3^p / \varepsilon_{cp}^p$ is used, with $\varepsilon_3^p =$ minor plastic strain.

The model behaviour in tension is linear elastic until the tensile strength f_t is reached (Fig. 3). Linear strain softening follows, governed by the normalized tension softening parameter $H_t = \varepsilon_1^p / \varepsilon_{tu}^p$ with $\varepsilon_1^p =$ major principal plastic strain (calculated from F_t) and $\varepsilon_{tu}^p =$ plastic ultimate strain in uniaxial tension.

$$f_{ty} = f_t \cdot \left(1 + \left(f_{tun} - 1\right) \cdot H_t\right) \tag{1}$$

ε_{tu}^p is derived from the fracture energy in tension, G_t and the characteristic length of the finite element, L_{eq}, which provides the necessary regularization to avoid mesh dependency of the numerical results. L_{eq} is calculated from the size of the finite element, A_{el}, and the number of stress points per element, n_{GP} (Pölling, 2000).

$$L_{eq} = 2\sqrt{\frac{A_{el}}{\sqrt{3} \cdot n_{GP}}} \tag{2}$$

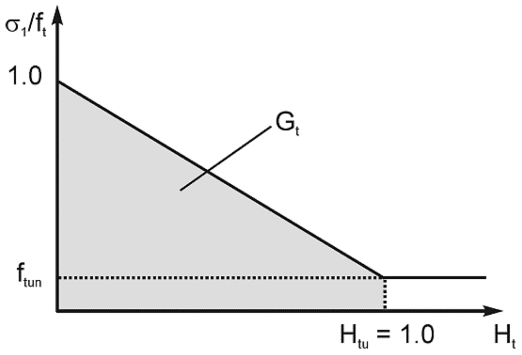

Figure 3. Normalized stress–strain curve in tension.

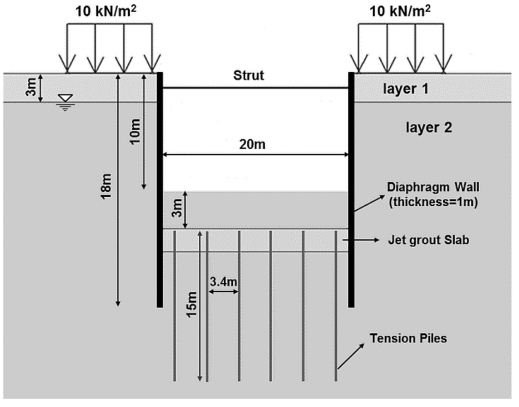

Figure 4. Layout of example analysed.

$$\varepsilon_{tu}^{p} = \frac{2 \cdot G_t}{(1 + f_{tun}) \cdot f_t \cdot L_{eq}} \tag{3}$$

Once the residual strength $f_{tu} = f_{tun} \cdot f_t$ is reached, no further softening takes place.

All other features, which essentially control the time dependent behaviour, are switched off for the purpose of this study and therefore from the parameter list given Table 1 only the Young's modulus, the Poisson's ratio, the compressive strength, the tensile strength, the residual tensile strength and the fracture energy in tension are required for the analysis.

3 APPLICATION TO PRACTICAL EXAMPLE

3.1 *Geometric layout*

The problem considered is a deep excavation with a jet grout slab constructed below excavation level. The slab is subjected to uplift pressure and thus additional tension piles are required (Fig. 4).

The main purpose of this contribution is to show that the newly developed constitutive model, originally proposed for modelling the mechanical behaviour of shotcrete, can be applied to solve this kind of problems, providing a better insight into the behaviour of jet grout panels under uplift pressure as compared to analyses where the jet grout material is modelled as linear elastic or perfectly plastic material without tension softening. Therefore the influence of different assumptions such as the fracture energy, the thickness and the shape of the slab on the results has been examined. Some consideration is also given to the behaviour of the slab in the vicinity of the diaphragm wall supporting the deep excavation.

Table 2. Parameters for the jet grout panel.

Name	Unit	Value
E_{28}	[GPa]	15
ν	[–]	0.2
$f_{c,28}$	[MPa]	8
$f_{t,28}$	[MPa]	0.8
f_{c0n}	[–]	0.7
f_{cfn}	[–]	1.0
f_{cun}	[–]	1.0
f_{tun}	[–]	0.05
$G_{c,28}$	[kN/m]	0.01 and 0.05

3.2 *Material parameters*

As mentioned previously the focus of the paper is on the mechanical behaviour of the jet grout slab and therefore only material parameters relevant for the slab are discussed here in detail. For soil layer 1 a simple Mohr-Coulomb failure criterion is assumed and for soil layer 2 the Hardening Soil model, a standard model in the Plaxis material models library is employed. The reason for choosing this model is that it takes into account the difference in stiffness between primary loadings and unloading/reloading, which is important in this particular case because a constant stiffness would overestimate the heave of the excavation base leading to higher bending moments in the slab and consequently the developments of crack patterns predicted would be unrealistic. For soil layer 2 a primary loading stiffness of 20 MPa and an unloading stiffness of 60 MPa has been assumed. The effective friction angle is 32.5° and effective cohesion is 0. The diaphragm wall is assumed as an elastic material. As mentioned above the time dependent development of strength and stiffness of the jet grout slab is not considered in this study because it is not relevant (the slab is stressed only after curing) but emphasis is put on the behaviour under tensile stresses. The relevant parameters are listed in Table 2. The analysis steps follow the usual procedure, i.e. initial stresses, walls wished-in-place, groundwater lowering and excavation in steps.

3.3 *Results-influence of connection slab/wall*

When constructing a slab with jet grout technology high pressures are involved and it can be expected that any residuals of slurry cake resulting from diaphragm wall construction will be cleaned off and therefore the

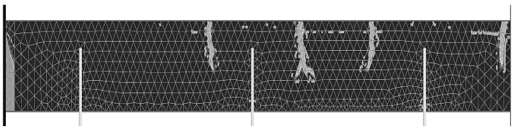

Figure 5. Crack pattern for reduced tensile strength near wall.

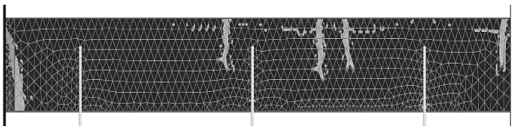

Figure 6. Crack pattern for full tensile strength near wall.

strength of the "interface" slab/wall will be relatively high and no distinct interface is created. To account for that in the numerical analysis no interface is placed between wall and slab but a small cluster is introduced where the tensile strength is reduced to 250 kPa. It follows from Figures 5 and 6 that this assumption has an influence on the crack development near the wall but the overall behaviour of the remaining slab is not affected significantly, keeping in mind that a numerical procedure involving tension softening is in general sensitive and therefore one should not put too much of interpretation on the exact position of individual cracks. It is also noted that this preliminary study has been performed with a slab thickness of 1 m which is not realistic from a practical point of view but has been chosen here to look at extreme conditions.

3.4 *Results-comparison with MC-model*

In this section the performance of a slab with 1.5 m thickness, which is more realistic from a practical point of view, is examined. The tensile strength in the cluster near the wall has been reduced to 250 kPa, otherwise the parameters listed in Table 2 apply, whereas $G_{t,28}$ is assumed to be 0.01 kN/m. Ideally, this value is determined from experiments (direct tension or bending test) but in practice this parameter will not be readily available in most cases. However, it can be assumed that the behaviour of jet grout material in tension is rather brittle, i.e. the stress strain curve shows a rapid loss of strength once the peak tensile strength is reached, i.e. the fracture energy is small. However, this will depend at least to some extent on the ground conditions. The consequences of this assumption are further discussed in section 3.5. In order to compare the results obtained with the new constitutive model with current practice, some analyses with a Mohr-Coulomb strength criterion without considering softening in the tensile regime for the slab have been performed.

Figure 7 depicts the obtained crack pattern and it follows that in the middle part of the slab cracks develop through about 2/3 of the thickness of the slab. Figure 8 shows a contour plot of the principal stress σ_3 whereas only tensile stresses are shown. The same is

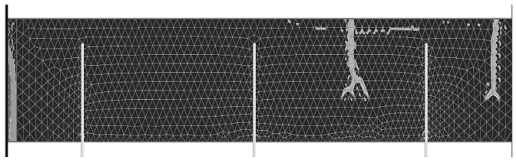

Figure 7. Crack pattern for slab with 1.5 m thickness.

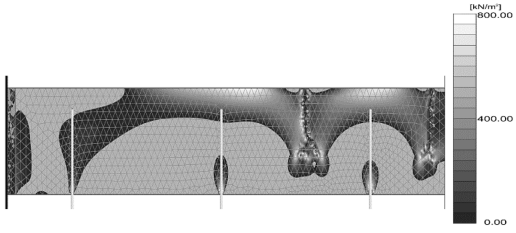

Figure 8. Contour plot of principal stress σ_3 (0–800 kPa) for slab with 1.5 m thickness.

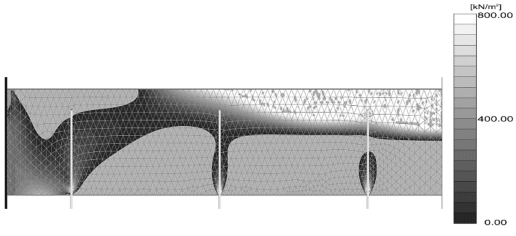

Figure 9. Contour plot of principal stress σ_3 (0–800 kPa) for slab with 1.5 m thickness – Mohr Coulomb criterion for slab.

plotted in Figure 9 for the analysis employing a Mohr-Coulomb criterion for the slab. It is clearly observed that stresses in the slab are significantly different because in a standard Mohr-Coulomb criterion the tensile strength can be limited but is not reduced to a residual value with the consequence that tensile stresses only develop through half of the slab thickness but remain at 800 kPa in a significant part of the slab. This is also reflected in Figure 10 where normal stresses are plotted in a cross section of the slab where a crack is present. With the new model the stress is zero but with the Mohr-Coulomb criterion the stress is 800 kPa (maximum tensile strength specified) and the depth of tensile stresses and cracks is much deeper with the new model. The same conclusion can be drawn from Figure 11 where bending moments are shown. It is evident that the bending capacity of the slab applying the Mohr-Coulomb criterion is significantly higher and is most probably overestimated.

3.5 *Results-influence of $G_{t,28}$*

In this section the influence of the assumed fracture energy in tension, which is required as input into the model, is investigated. Based on sparse available data from projects and experiments (mainly for concrete though) values for $G_{t,28}$ can be suggested to be in

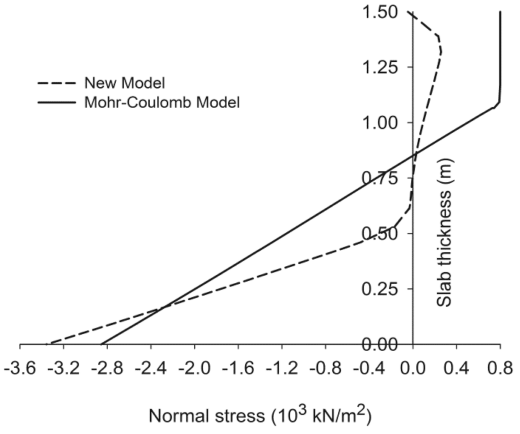

Figure 10. Comparison of normal stresses across slab.

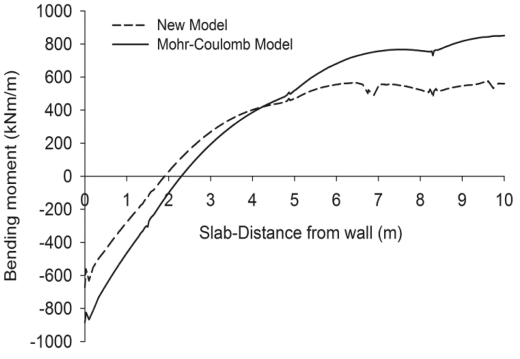

Figure 11. Comparison of bending moments in slab.

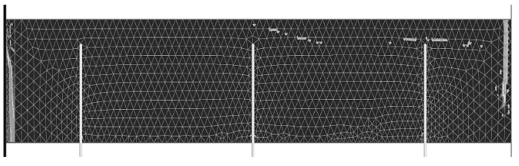

Figure 12. Crack pattern – $G_{t,28} = 0.05$ kN/m.

the range of 0.01 to 0.05 kN/m, the lower value being more likely to be representative and therefore this has been assumed as basis for results presented in the previous chapter. If the input for the fracture energy is increased to 0.05 kN/m, representing a very ductile behaviour, the crack pattern obtained is shown in Figure 12 which has to be compared to Figure 7, where the same is plotted for $G_{t,28} = 0.01$ kN/m. Figure 13, to be compared with Figure 8,shows a contour plot of the principal stress σ_3 and again only tensile stresses are shown. The differences are obvious. Although the maximum tensile stress is reached towards the center in the upper third of the slab, cracks do not develop deeper because softening is less severe and equilibrium can be established. However significant cracking occurs at the connection to the diaphragm wall and in

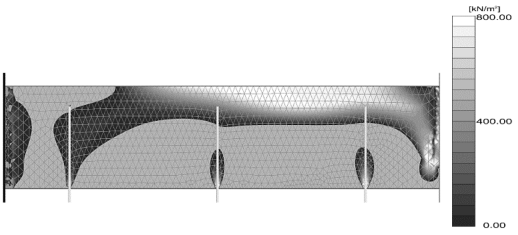

Figure 13. Contour plot of principal stress $\sigma_3 - G_{t,28} = 0.05$.

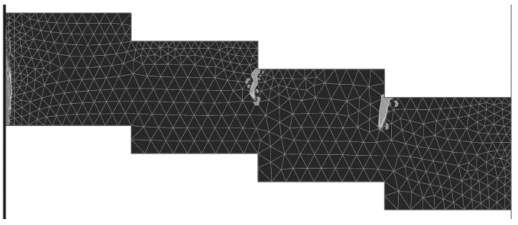

Figure 14. Crack pattern – no tension piles.

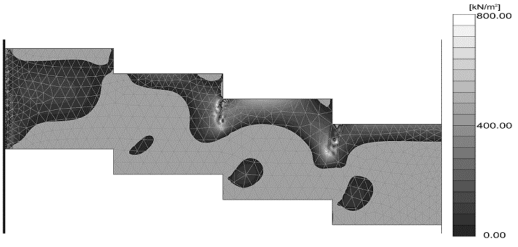

Figure 15. Contour plot of principal stress σ_3 – no tension piles.

the center of the slab, very similar to the analysis with $G_{t,28} = 0.01$ kN/m.

3.6 *Results-influence of slab geometry*

All analyses presented so far are with tension piles in place as indicated in Figure 4. As construction of these tension piles is a significant cost factor it is investigated whether or not a different geometry of the jet grout slab, namely in form of a staggered arch, would be a feasible alternative. The individual sections have a thickness of 2 m, i.e. the overlap at the boundary of the sections is 1.5 m (see Figure 14). The numerical analysis shows that it is indeed possible to achieve equilibrium with this system. The crack pattern obtained follows from Figure 14 and the contour plot of σ_3 from Figure 15. Cracks develop at the boundary of the sections and near the wall.

Because of the high compressive forces in the upper part of the slab at the connection to the wall an additional analysis has been performed, not only reducing the tensile strength in a cluster adjacent to the wall (to 250 kPa) but also the compressive strength (to 2500 kPa). The effect follows from Figures 16 and 17 which show the distribution of normal and

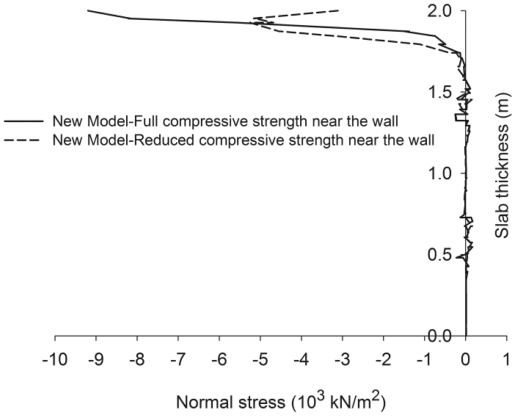

Figure 16. Comparison of normal stresses across slab near wall.

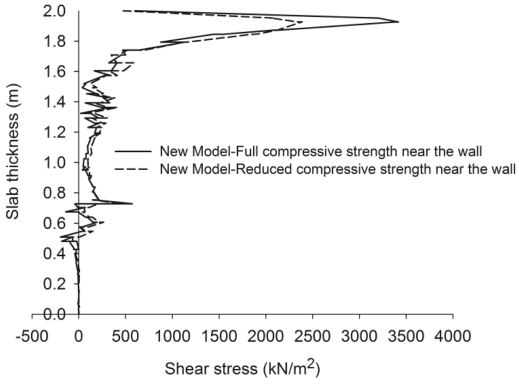

Figure 17. Comparison of shear stresses across slab near wall.

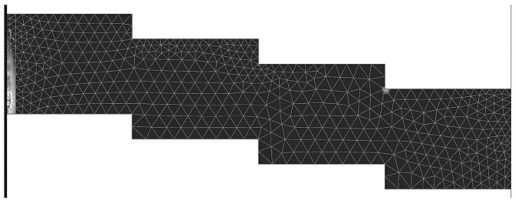

Figure 18. Crack pattern – $G_{t,28} = 0.05$.

shear forces along a cross section in the vicinity of the wall. The crack pattern does not change notably due to this assumption.However, assuming a fracture energy of $G_{t,28} = 0.05$ kN/m, i.e. assuming a more ductile behaviour, reduces cracks significantly, as follows from Figure 18.

4 CONCLUSIONS

In this paper a constitutive model, originally developed for modelling the mechanical behaviour of shotcrete, has been applied to model the behaviour of a jet grout panel, constructed below the base of a deep excavation to provide resistance against uplift pressure. Emphasis was put on the behaviour after reaching the tensile strength of the material. It could be shown that significantly different results with respect to the stress distribution in the slab are obtained as compared to modelling the behaviour of the slab with a simple Mohr-Coulomb failure criterion with tension cut-off. Although no direct comparison with measurements is possible it can be postulated that qualitatively realistic crack patterns are obtained. The influence of different assumptions such as the value chosen for fracture energy has been addressed. It could be shown that for a favorable geometry of the slab the tension piles could be omitted.

REFERENCES

Arroyo, M., Ciantia, M., Castellanza, R., Gens, A. & Nova, R. 2012. Simulation of cement-improved clay structures with a bonded elasto-plastic model: A practical approach. *Computers and Geotechnics*, 45: 140–150.

Borchert, K.-M., Henke, S. & Richter, T. 2013. Die Düsenstrahlsohle als horizontales Aussteifungselement. *In Proceedings Workshop Bemessen mit Numerischen Methoden* (Grabe, editor), Hamburg Harburg, 24.–25.9.2013, 198–220.

Brinkgreve, R.B.J., Engin, E. & Swolfs, W.M. 2012. Finite element code for soil and rock analyses. Users Manual. Plaxis bv, The Netherlands.

Fang, Y.-S., Liao, J.-J. & Sze, S.-C. 1994. An empirical strength criterion for jet grouted soilcrete. *Engineering Geology*, 37: 285–293.

Gens, A. & Nova, R. 1993. Conceptual base for a constitutive model for bonded soils and weak rocks. In *Proceedings of the international symposium on Geotechnical Engineering of hard soils-soft rocks*, Athens, 485–494.

Horpibulsuk, S., Liu, M.D., Liyanapathirana, D.S. & Suebsuk, J. 2010. Behaviour of cemented clay simulated via the theoretical framework of the Structured Cam Clay model. *Computers and Geotechnics*, 37: 1–9.

Kudella, P., Mayer, P.-M. & Möller, G. 2003. Testing and modelling the ductility of buried jetgrout structures.In O. Natau, E. Fecker, E. Pimentel (eds.) *Proc. Int. Symp. GeoTechnical Measurements and Modelling (GTMM)*, Karlsruhe. Rotterdam: Balkema

Pölling, R. 2000. Eine praxisnahe, schädigungsorientierte Materialbeschreibung von Stahlbeton für Strukturanalysen. PhD thesis, Ruhr-Universität, Bochum.

Schaedlich, B. & Schweiger, H.F. 2014. A new constitutive model for shotcrete. *Proc. 8th Eur. Conf. Num. Meth. Geot. Eng.,* Delft, 18.-20.6.2014, accepted for publication.

Yu, H.S. 1998. CASM: a unified state parameter model for clay and sand. *Int. J. Numer. Anal. Methods Geomechanics*, 22: 621–653.